

Fundamentals, topologies and optimization methods of saturated iron core fault current limiter

ABSTRACT

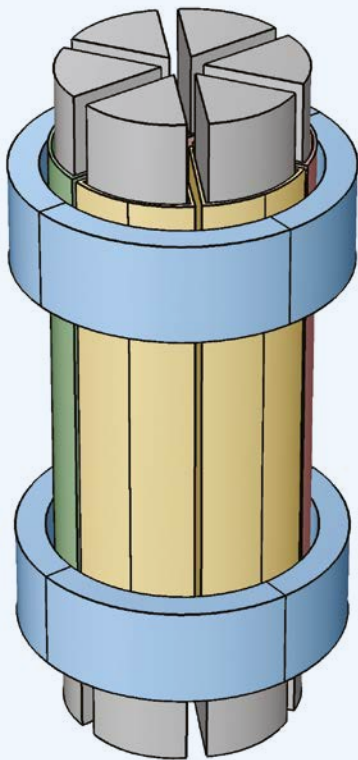
The energy transition is a necessity to satisfy the consumption and impact of humanity on the environment. Therefore, to fulfill this demand, renewable energies and microgrids have been developed. Consequently, fault current levels have overcome the circuit breaker capacity in many substations over the years. Then, the development of the fault current limiters has become a potential solution to solve this problem. The literature has presented several topologies over the past decades.

The saturated iron-core fault current limiter (SIC-SFCL) has exhibited promising results since this topology is tested in the distribution and transmission system substation. Thus, enforcements to increase the maturity of this equipment have been developed in different areas, for example, design, applied superconductor materials, and optimization models of the SIC-SFCL. This article has presented the fundamental concept of this equipment. Beyond that, the principal topologies have been discussed. The article has delivered further information

about the main parts that comprise this equipment. Also, the authors have introduced different characteristics which affect the recovery times of this device. The authors have discussed the optimization methods applied to this equipment and after the conclusion is presented.

KEYWORDS

design, fault current limiter, operation principles, design, optimization, saturated iron core superconducting fault current limiter



1. Introduction

Due to the increase of the power demand together with the distributed power generation, the level and frequency of short circuit faults have increased. The traditional solution, which mitigates this problem, has become obsolete. Due to the fact, the fault current limiters (FCL) have been presented as a potential solution to solve this problem properly. Over the years, many topologies have been presented, for example, resistive superconducting FCL (R-SFCL), power electronics FCL, shielding superconducting FCL, and saturated iron core superconducting FCL (SIC-SFCL) [1]–[6].

The literature has studied SIC-SFCL prototypes deeply among these aforementioned groups where this topology was tested in the live grids. For example, in [7]–[10], the authors have presented the 35 kV/90 MVA SIC-SFCL installed in the Puji substation. In [11]–[13], the 220 kV/300 MVA was developed and tested in the live grid. Due to this, this topology has proved the potential to be a commercial and suitable solution to short circuit problems. More recently, in

Due to the increase of the power demand together with the distributed power generation, the level and frequency of the short circuit faults have increased

[14]–[18], the authors have exhibited a design, simulation, and manufacturing of an SCI-SFCL of 500 kV. Furthermore, other topologies presented in the literature have had auspicious results. For example, several groups have analyzed the open core fault current limiter [19]–[23]. Antonio Pellicchia et al. presented in [20] the 33 kV/800 A open-core saturated fault current limiter, which was tested in the real short-circuit situation.

Also, several research groups have investigated the analytical and numerical method to represent characteristics of this equipment in the power electrical grid. In [24] N. Vilhena et al. have presented a methodology to model the dynamic behavior of the SIC-SFCL with a lumped electrical circuit. In [25] the authors have considered the influence of the SIC-SFCL inserted in the power transmission line.

As presented in the aforementioned articles, the SIC-SFCL has demonstrated a promising ability to act in several areas of the power electrical system, such as distribution and transmission lines. Therefore, understanding better the behavior of this equipment is fundamental to placing the SIC-SFCL on the market.

This article introduces the fundamental principle of this SIC-SFCL, where different topologies are presented and discussed, the main parts comprising the SIC-SFCL are discussed. Furthermore, the recovery time of this equipment is introduced and analyzed to different iron core materials. Finally, optimization solutions for the iron core and the

superconducting coil have been presented.

1.1 Fundamental principals and topologies

This section explains the fundamental principles of the SIC-SFCL. It is focusing on the general concepts of this equipment, describing the SIC-SFCL behavior in steady-state and short-circuit regimes.

Fundamentally, the SIC-SFCL is composed of iron cores, the AC coils are generally made of copper, and the superconducting material is used for the DC coils. Regardless of topology, the SIC-SFCL works on two different conditions: the steady-state or short-circuit regimes. The equipment idea centers on saturation and desaturation of the iron core. In the steady-state regime, a DC magnetomotive force (MMF_{DC}) is greater than the AC one. Consequently, it leads the SIC-SFCL to the saturating region of the ferromagnetic material. On the other hand, in the short-circuit period, the AC magnetomotive force (MMF_{AC}) overcomes the DC one. As a result, the operation point of the SIC-SFCL goes out to the ferromagnetic material linear region.

Fig. 1 illustrates the explained concepts above. In the steady-state regime, the DC current drives a MMF_{DC} greater than the MMF_{AC} . It implies that the dominant magnetic flux density comes from the DC part. Dot green in Fig. 1 represents the steady-state operating point. When short-circuit happens, the AC current increases as well as the MMF_{AC} . This fact leads the operating point to the linear region of

The SIC-SFCL is composed of iron cores, the AC coils are generally made of copper, and the superconducting material is used for the DC coils

When the short-circuit occurs, one iron core desaturates, and the inductance of the AC coils increases, thus providing the reduction of the short circuit current

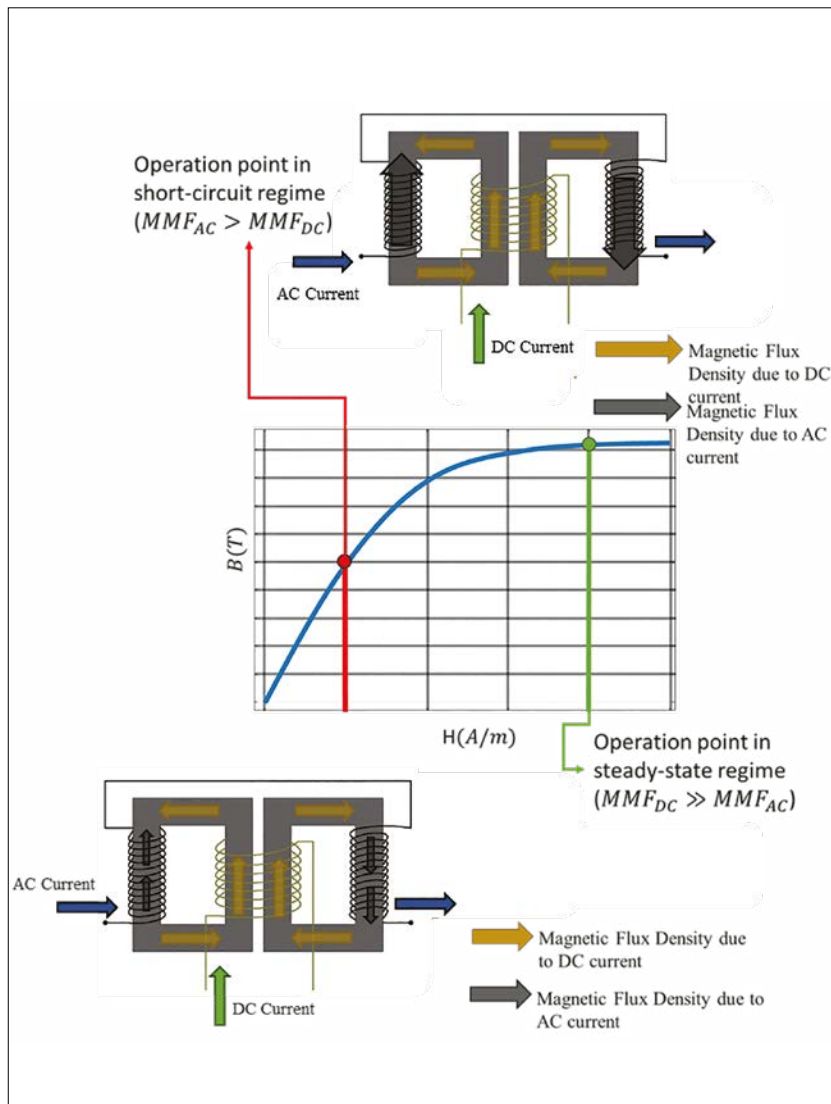


Figure 1. The SIC-SFCL behavior in the steady-state and short-circuit regimes

the ferromagnetic material. The red dot represents the short-circuit operating point.

In the SIC-SFCL, the AC coils (in black color in Fig. 1) are wound in the opposite direction making the AC magnetic flux circulate the reverse-path inside in the different iron cores. On the other hand, the DC superconducting coil (in gold color in Fig. 1) generates a third magnetic flux, which goes in the same direction in both iron cores. In the steady-state regime, the superconducting DC coil has a small induced voltage due to the same

magnitude and the reverse direction of the AC magnetic fluxes. In contrast, when the short-circuit occurs, one iron-core desaturates, and the other one saturates even more. Equation (1) shows the inductance to the SIC-SFCL for both situations. Where the L_{ac} is the inductance of the AC coils, the A_{ac} is the cross-section area of the legs where the AC coils are placed, the N_{ac} is the number of turns of the AC coil, the l_{mean} is the mean length of the AC magnetic flux path, and the B, H is the magnetic flux density and the strength of the magnetic field, respectively. Also, it is possible to see in equation (1) that the

derivation dB/dH represents the magnetic permeability (μ), which is given by the slope of the curve at the operating point.

$$L_{ac} = \frac{A_{ac}N_{ac}}{l_{mean}} \frac{dB}{dH} \quad (1)$$

This scenario provokes a fast change of the magnetic flux through the DC coil. Then, as predicted by the Maxwell equations a high induced voltage appears between the DC coil terminals. This high voltage can revert the DC current direction and damage the power supply. As an example, Fig. 2 presents an induction voltage and current for a 220 V/30 A 3D simulated SIC-SFCL at the three-phase short-circuit and the distortion of the magnetic flux density at 18 ms of the simulation. It is observed before the short-circuit, the current applied on the DC superconducting coil is equal to 250 A. Moreover, the voltage drop across the DC coil terminals is nearby zero. However, at the short-circuit regime, the first peak of this induced voltage is close to the RMS voltage line. As a protective way, a fast switch is placed between the power supply and the DC coil. When the short circuit happens, the fast switch opens the circuit. Another protection is a shunt resistor that is used to limit the induced current and to dissipate the energy of the DC coil.

1.2 Iron-cores topologies of SIC-SFCL

The literature presents different iron-cores topologies for the SIC-SFCL. This section will present and discusses them, where their advantages and disadvantages will be highlighted. For all figures, the same legend for separating the phase coils is used. The yellow, red, and green colors represent phases A, B, and C, respectively, for the AC coil, and the blue color represents the DC ones.

Fig. 3 presents a topology of the SIC-SFCL widely studied in the literature. It has six iron cores, each having a copper coil wound in the outermost limbs of the iron core. Two iron cores and copper coils form one phase of the power electrical system, while the same phase coils are located on diametrically opposite sides. In contrast, the DC coil is wound around all the inner iron-cores limbs, providing for the six iron cores DC magnetic field, which deeply saturates cores. This topology can limit all short-circuit types. The Innopower group has extensively studied

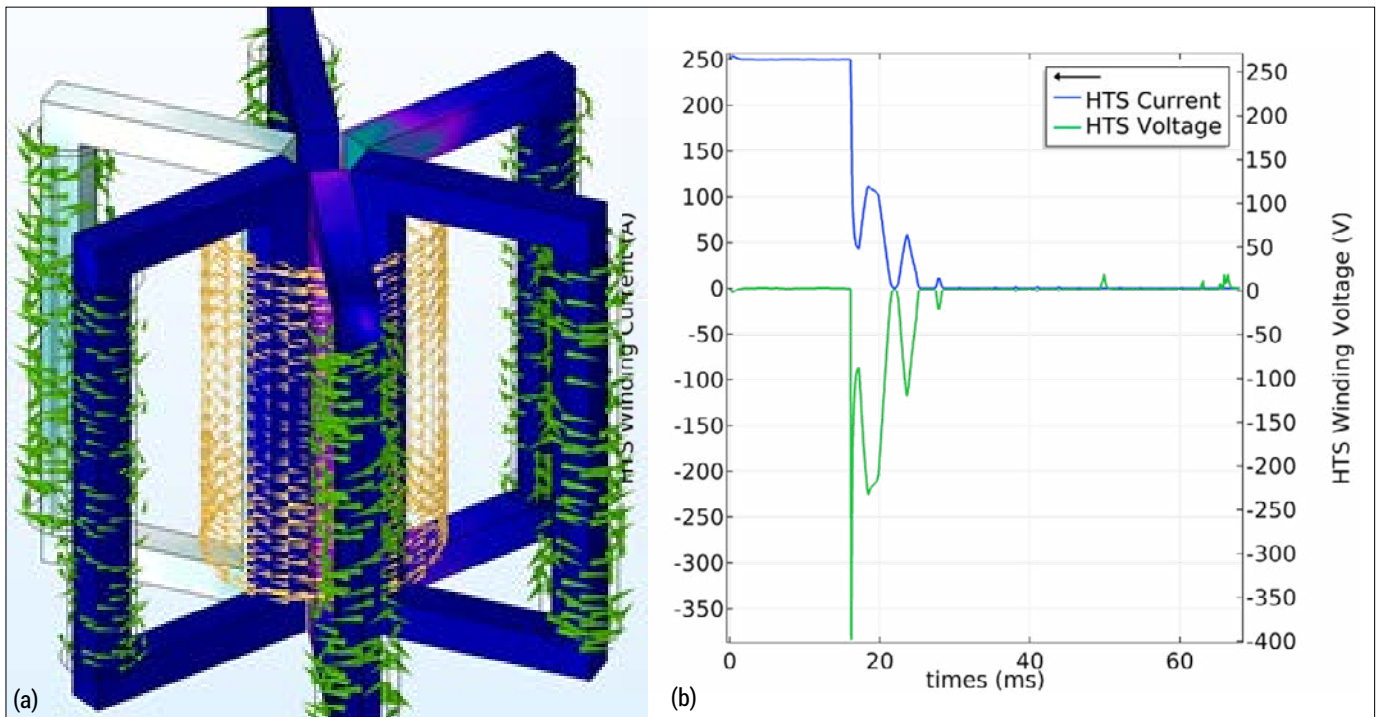


Figure 2. (a) SIC-SFCL six-leg in transient period (b) current and voltage of the DC coil in the transient period

this topology. The first one has voltage and power ratings of 35 kV and 90 MVA [10]. The second prototype has 220 kV and 300 MVA [13]. Both were tested in the real power electrical grid. Moreover, the Electric Power Research Institute, Guangdong Power Grid has developed a 500 kV SIC-SFCL six legs prototype to be installed in the China transmission grid [14]. Moreover, this topology has reached a high-voltage level, showing the capability to work in the power transmission and distribution systems. Furthermore, this topology does not pose a security risk. It means that even without the DC current, the equipment keeps working. Its disadvantage is the large size and weight. In the next sections, methods that could reduce the iron-core material will be presented.

Fig. 4 shows the three-leg topology of the SIC-SFCL. Using this configuration, it is possible to reduce the mass and the volume of the iron-core. However, this topology uses two DC coils, which are wound in opposite directions. Each DC coil is placed in one of the outermost limbs (left and right side). This configuration performs a path for the DC magnetic flux, which is responsible for the deep saturation of the iron-core. In this case, the AC coils are wound in the same direction and are connected in series, where it provides an open path for the AC flux through the outermost limbs. In

The six-leg topology of SIC-SFCL can limit all short circuit types, it has been successfully implemented in China, but it uses more materials compared to the other topologies

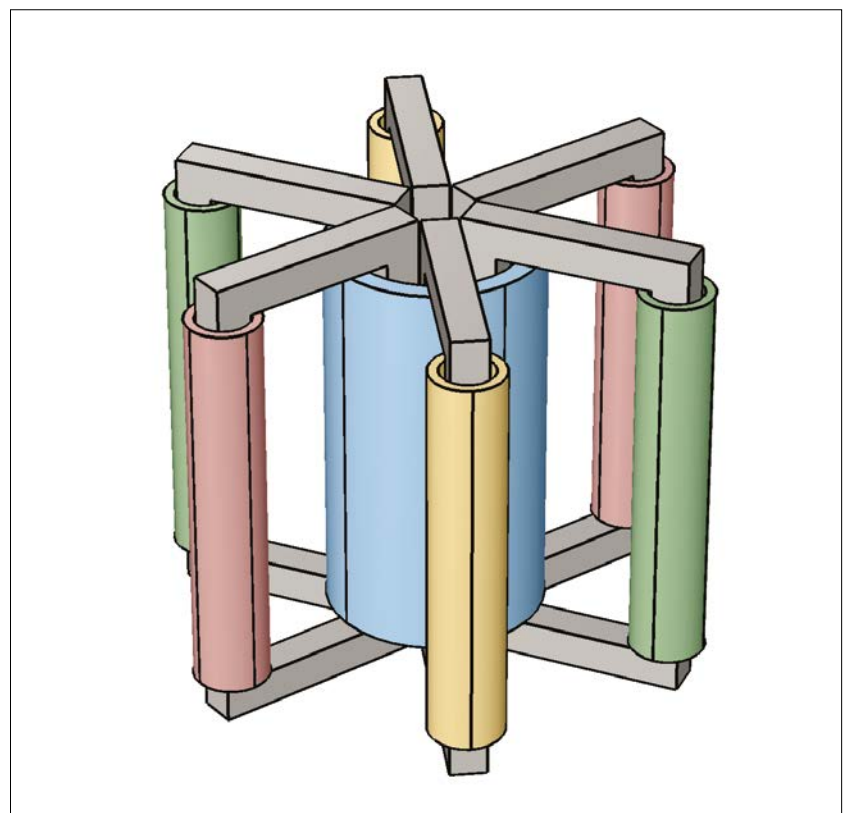


Figure 3. SIC-SFCL six-legs

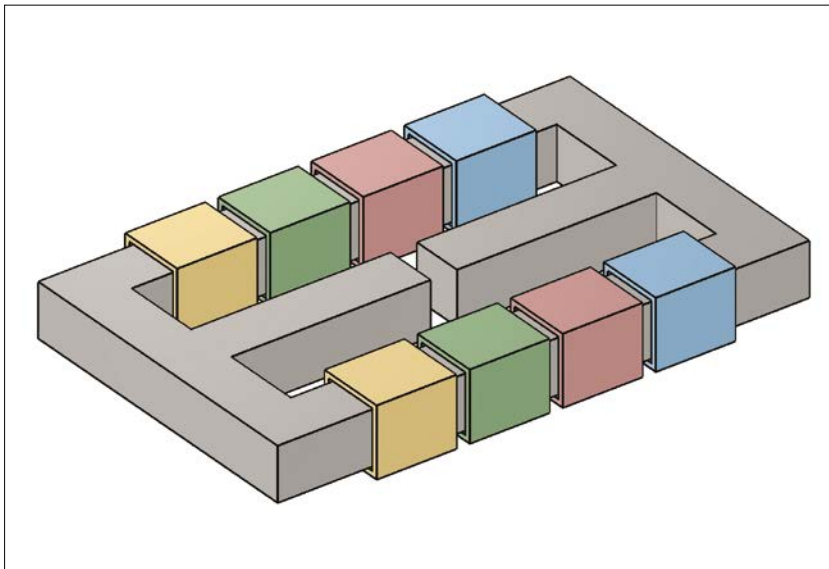


Figure 4. SIC-SFCL three-leg

The three-leg topology has a strong AC magnetic coupling due to the location of the AC coils, which means that regardless of the short-circuit type, all phases will be affected by a fault

this configuration of the coils, when the short-circuit happens, each limb is alternately desaturated.

It is important to include an air gap in the middle of the central limb because of the arrangement of the DC coils, thus allowing the DC magnetic flux to flow dominantly in the outermost limbs. Moreover,

the air gap provides a way to the AC magnetic flux without affecting the DC one. Then, in this configuration, the central limbs make a parallel way that decouples the AC and DC magnetic flux. In addition, the central limbs need to be twice as large compared to the outermost limbs. It provides a proper and effective limitation in the short-circuit condition [26].

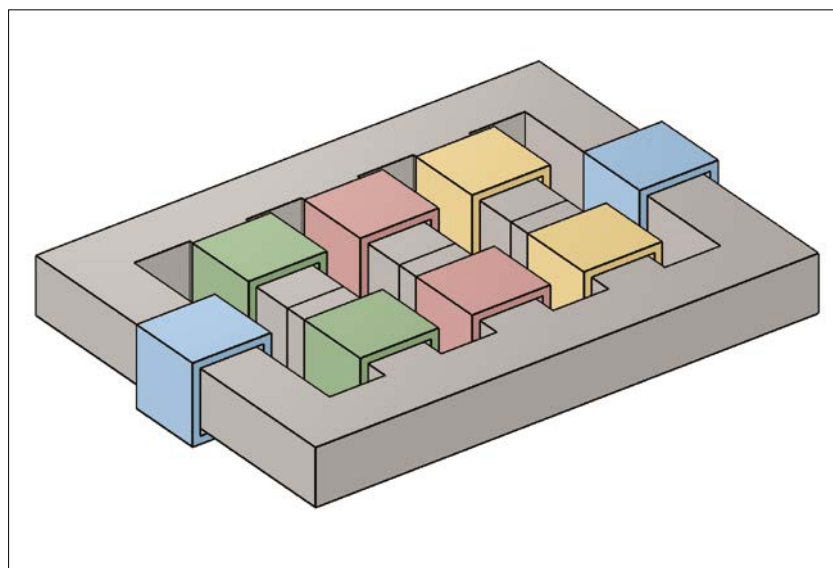


Figure 5. SIC-SFCL five-leg

For this topology, equation (2) expresses the AC inductance, where the l_{gap} and μ_r mean the gap of the central limbs and the relative magnetic permeability.

$$L_{ac} = \frac{A_{ac}N_{ac}}{l_{mean} + \mu_r l_{gap}} \frac{dB}{dH} \quad (1)$$

This topology has a strong AC magnetic coupling due to the location of the AC coils, which means that regardless of the short-circuit type, all phases will be affected by a fault.

Fig. 5 shows the five-leg SIC-SFCL topology. An advantage of this topology is the magnetic decoupling of the AC coil. Different from the topology in Fig. 3, this one separates each phase of the AC coils in specific limbs. The DC coil is placed in the outermost limbs on the left and right sides. This topology is able to limit all short-circuit types. However, the unsymmetrical faults generate a zero sequence of magnetic flux. Then this one returns by the external path, where the DC coils are placed. The demagnetization of the outermost generates a high zero sequence reactance. Then the zero-current sequence is smaller. On the other hand, when the symmetry short-circuit happens, the no-zero sequence is generated. To reduce the hysteresis losses, it is possible to use the air gaps in the five-leg SIC-SFCL. However, it is important to notice that these air gaps increase the coupling between the coils.

Fig. 6 presents the open-core SIC-SFCL. This topology utilizes six open iron cores, where each one has an AC coil. Two AC coils of the same phase can be oppositely wound and connected in series. Different from the other shown FCLs, this one has a triangular cross-section. Moreover, this topology has two DC coils, which are wound in the same direction providing

Open core topology utilizes six open iron cores, each having an AC coil, where two AC coils of the same phase can be oppositely wound and connected in series

the deep saturation of the iron cores. For practical application, the six iron cores need to be immersed in an oil tank. It furnishes suitable insulation and cooling. The radiator provides natural convection, which implements the cooling process without the need for the forced ventilation.

In [20], A. Pellecchia et al. developed an open-core SIC-SFCL with a 45 MVA/33 kV-800 A rating. The superconducting DC coil was built by a multi-filament of magnesium diboride (MgB_2). To encapsulate the DC coils, epoxy resin was used. The development of these DC coils occurred in Genoa, Italy. The operating temperature of these coils is set up to 16 K. Strong advantage of this topology is a reduction in the induced voltage inside of the DC coils during the transient periods.

2. The main components of the SIC-SFCL

In the practical application, the SIC-SFCL is composed of major parts. This section will present and discuss these different parts.

2.1 The superconductor DC coil

One of the main parts of the SIC-SFCL equipment is a superconducting coil. It provides a deep saturation of the iron cores in a steady-state regime. As was briefly presented in section 2, the high-temperature superconductor (HTS) coils have distinct topology and materials. In this section, the HTS wires and tapes used traditionally to develop the high voltage and power SFCL will be discussed.

In [27], the authors present a 35 kV/90 MVA SIC-SFCL, and its DC HTS coils are constructed with Bi2223/Ag tapes. The HTS coils were built with 44 double pancake rings and 470 turns. This configuration gives a 141 kA-turn, where the DC voltage and current applied were equal to 50 V and 350 A in the steady-state regime.

In [12] a 220kV/300 MVA SIC-SFCL has been developed, and its superconducting DC coil was composed of Bi2223 with 2520 turns, where 9 rings of 56 turns were connected in series, creating a group, and five groups were connected in parallel. The critical current density range of the tape was equal to 140-180 A, in self-field 77

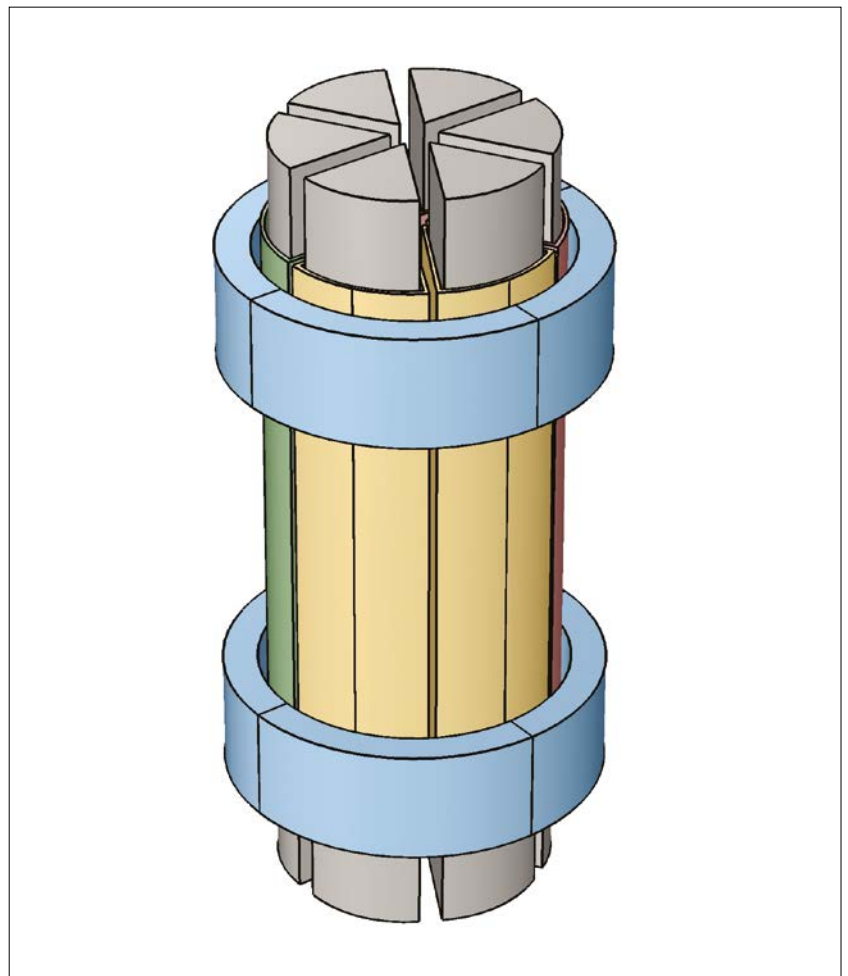


Figure 6. Open-core SIC-SFCL

One of the main parts of the SIC-SFCL equipment is a superconducting coil which provides a deep saturation of the iron cores in a steady-state operation

K. The DC current applied in each group was equal to 60 A, then the total current requested to the source is equal to 300 A.

In [16], the authors show a design of a 500 kV HTS DC coil of a single-phase SIC-SFCL. In this project, the HTS coil was constructed with two HTS materials, Bi-2223 and YBCO. The YBCO and Bi-2223 pancake coils are equal to 8 and 80. Moreover, the coil turns series-connected are 208 and 416, respectively. The YBCO is placed in the upper and lower position of the HTS coil, and the Bi-2223 is located in the middle of the coil. Moreover, there are two sources to supply the HTS coils. The YBCO and Bi-22230 are supplied with 160 A and 560 A, respectively.

An important aspect that should be mentioned is the influence of the perpendicular magnetic field over the HTS coil. Fig. 7 illustrates this phenomenon. When the iron cores are deeply saturated, some part of the magnetic flux disperses out of the core. This dispersion of the magnetic flux reaches the superconducting coil and affects the critical current density of the material, reducing the current capacity of the HTS coil. This fact influences the superconducting coil design, where an optimal place is required to maximize the HTS coil critical current density [6].

In [28], the authors have studied the influence of the DC current in HTS coil losses at the steady-state regime. It was observed

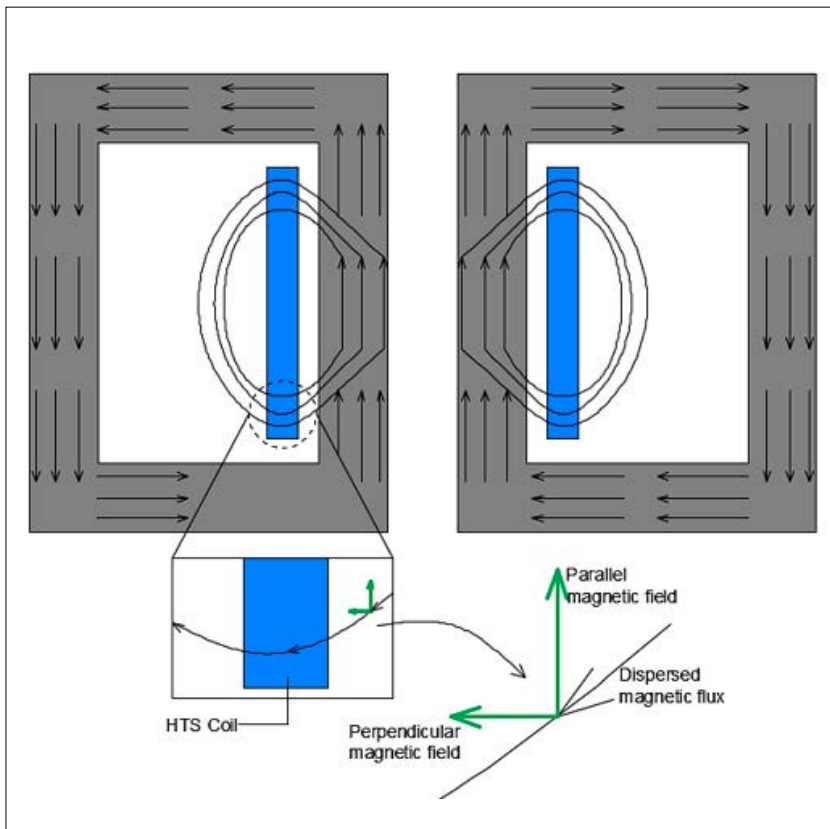


Figure 7. Dispersed magnetic flux over the HTS coil

The cryogenic system is required to lead the HTS coils to the superconducting state, and it commonly uses liquid nitrogen

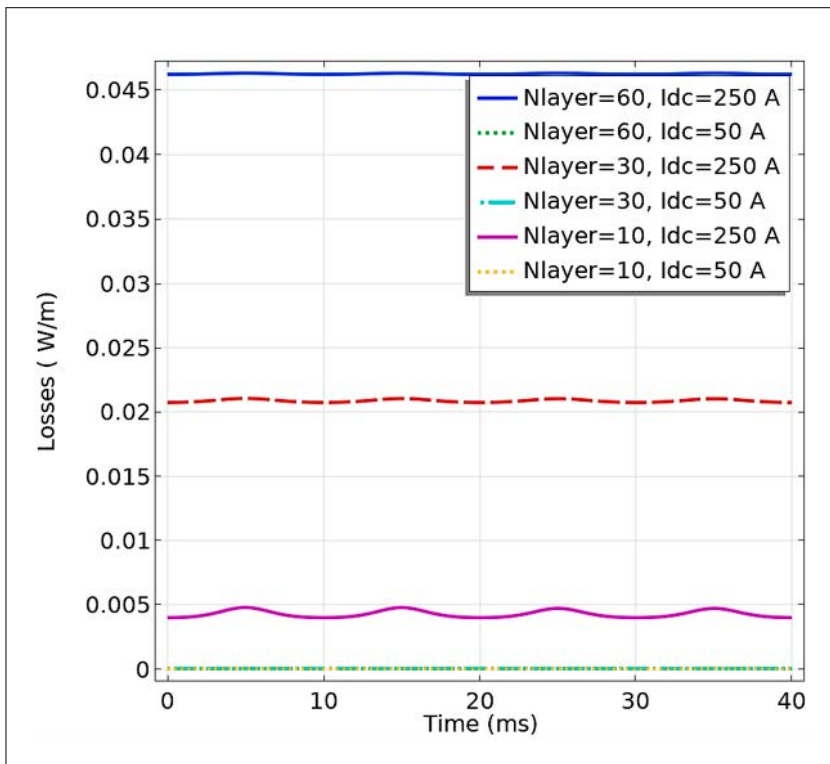


Figure 8. HTS coil losses due to the different

generates its losses [29]. Fig. 8 presents the power losses at the steady-state regime calculated for different applied DC current and configurations of the HTS coil. Regarding the configuration of the coil, the number of the turns was kept constant equal to 60, and the number of layers was varied between 60, 30, and 10. As possible to see by Fig. 8, the power losses rise as the applied current, and the number of the layers increase.

2.2 Cryogenic system for HTS coil

The cryogenic system is required to lead the HTS coil to the superconducting state. This system is composed of current lead, insulators, refrigerator substance inlet and outlet, temperature and pressure sensors, a Dewar, a refrigeration substance tank, and a control unit. The current lead makes the connection between the DC power supply and the superconducting coil. The insulators guarantee the cryogenic temperature in the Dewar that hosts the HTS coil and the refrigeration substance. The material to build the Dewar needs to minimize the eddy currents, which is the reason why the nonmagnetic 304 stainless steel is a commonly used material. The control unit is used to control the pressures, the refrigeration substance capacity, as well as for the control of the valves and pumps between the tank and the Dewar. Commonly, liquid nitrogen (LN₂) is used to keep the HTS coil to the superconducting state. Fig. 9 summarizes the cryogenic system.

2.3 AC coils and the Oil tank

The AC coils are commonly made of copper material. The winding direction of one phase can be in the same or in the opposite direction, and it depends on the topology. In the high voltage system, an

The magnetization system is responsible for driving the SIC-SFCL to the saturated point in the steady-state operation, and it needs to cut off the magnetization in the fault occurrence as quickly as possible

important aspect to consider is the capacitance between the turns of winding [11]. In these cases, the oil tank hosts the AC coils and is responsible for the AC coils insulation.

Furthermore, in the case of high voltage, three separate oil tanks are preferred than integrated ones, avoiding possible additional difficulties in the assembly of the equipment. For example, the single oil tank structure implies that iron cores must install inside the oil tank. Moreover, the Dewar hosting the HTS coil also being inside the oil tank. It creates a highly problematic or impossible assembly structure. Due to the separation of the iron cores, an important aspect in the construction of the tank is non-metallic material. It will prevent eddy currents that would heat and generate losses in the walls of the oil tank.

2.4 Magnetization system

The magnetization system is responsible for driving the SIC-SFCL to the saturated point in the steady-state regime. Furthermore, this system needs to be capable of cutting off the magnetization in the fault occurrence as quickly as possible. Moreover, a quick recovery is required of the system, where a high impedance state turns to a low impedance when the fault is extinguished. The magnetization system consists of three parts:

- DC superconducting coil
- protection system
- rectifier system

The protection system has a structure for avoiding the HTS coil damages, composed of the energy release circuit and a power electronic switch. The energy release acting in the first instant of the fault guarantees that the induced voltage in the HTS coil does not damage it. Generally, a ZnO piezo resistor is used in this system. The power electronic switch is responsible for turning off the current from the source and avoid a reversible current from the HTS coil to the DC power source. Fig. 10 shows a schematic of the SIC-SFCL with the DC power supply and the protection system. The switch S_1 represents the power electronic fast power switch. The diode D_1 and the resistance R_{shunt} represent a protection system, and the current source represents the power supply with a controlled current.

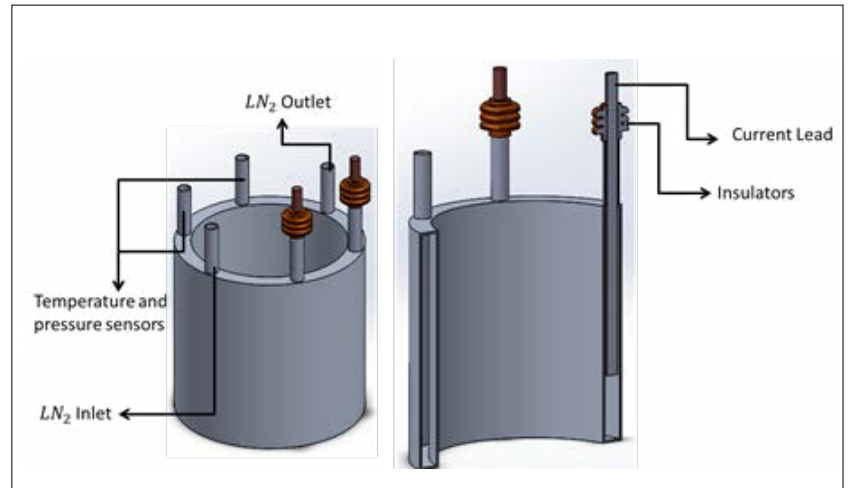


Figure 9. Cryogenic system

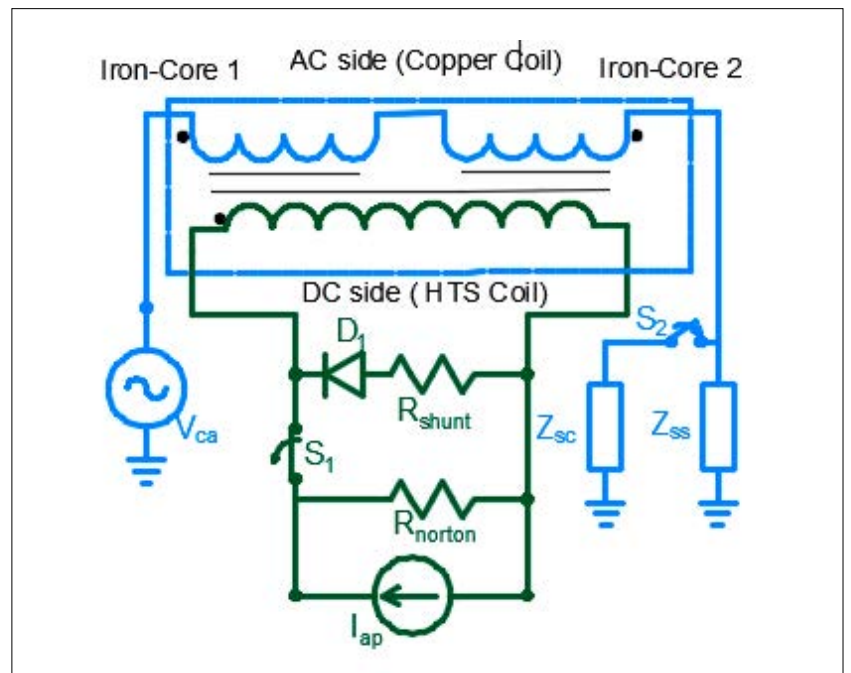


Figure 10. The schematic of the SIC-SFCL with the DC power and protection system

After the fault clearance, the iron core needs to be re-saturated to get back to the low impedance state – the time required for that operation is called SIC-SFCL recovery time

3. SIC-SFCL recovery time

After the fault clearance, the iron core needs to be re-saturated for the fault current limiter to turn to the low impedance. This re-magnetization should occur after the circuit breaker opens the power line in the fault. Then the SIC-SFCL has the re-closing time as a maximum time to be re-saturated. Two aspects that could highly impact the re-

covery time are the lamination of the iron cores sheet and the material used to build the cores. Fig. 11 presents in (a) the magnetic flux density of the iron cores in the transient period and in (b) the same quantity in the steady-state regime. Moreover, in Fig. 11(c), the DC current transient behavior of four different iron core materials is compared. This result shows the iron core impact on the re-saturation process.

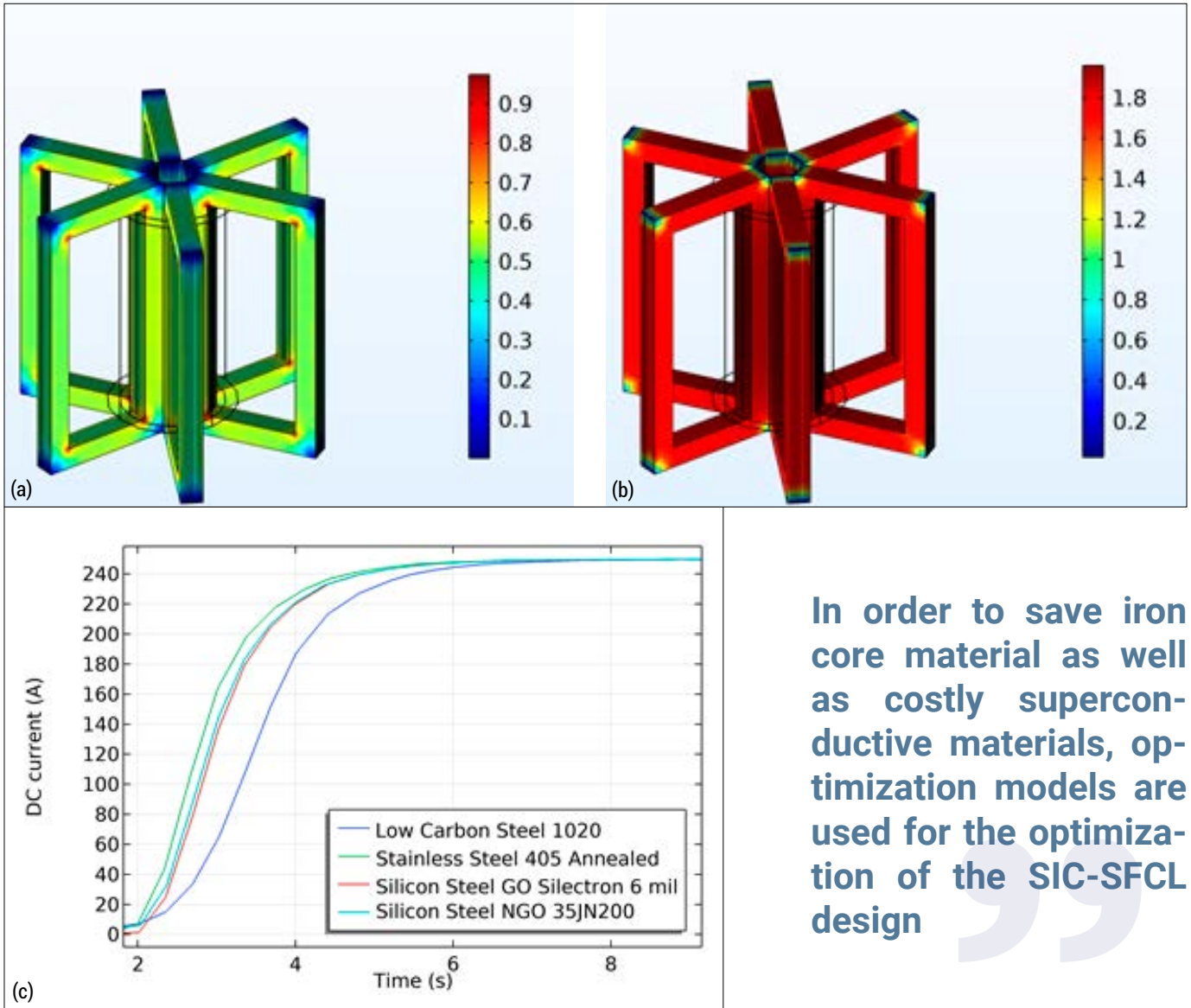


Figure 11. (a) Transient period of the re-saturation of the iron-cores of the SIC-SFCL; (b) Steady-state regime after the saturation process of the iron-cores of the SIC-SFCL; (c) DC current transient behavior to different iron-cores materials

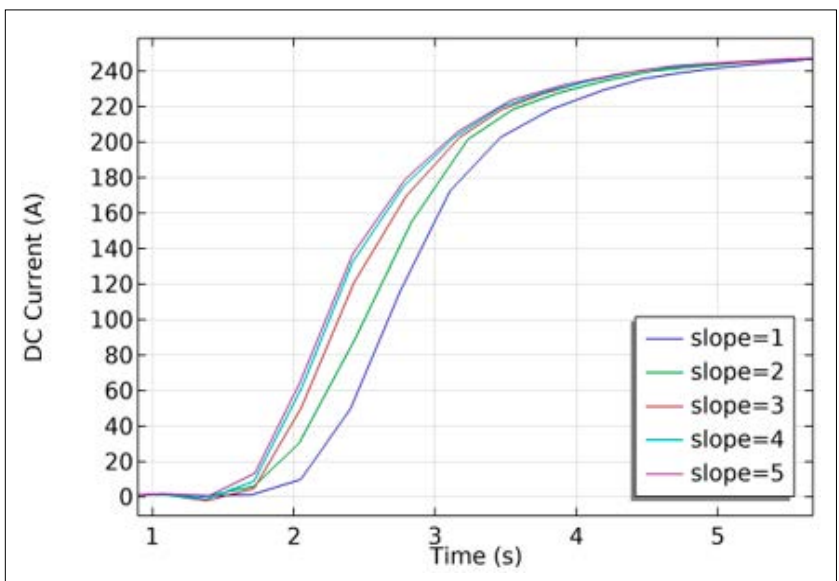


Figure 12. The transient behavior of the DC current due to different slope in the voltage power source

In order to save iron core material as well as costly superconductive materials, optimization models are used for the optimization of the SIC-SFCL design

Furthermore, the current shape applied to the HTS coil can be efficiently designed to magnetize the superconducting coil. A fast magnetization is important to restore the saturated state before the re-closing of the circuit breaker. Fig. 12 shows different DC current applied into DC coil and compares the transient DC current behavior. For the presented Fig. 12, a DC voltage source applied the proper voltage to generate the 250 A in the steady-state regime. The shape of the voltage source was the ramp function, where the slope of this ramp could be changed.

4. SIC-SFCL optimization models

Another important subject of this fault current limiter is the amount of iron core material used in its construction. Further, the HTS and the cooling system contribute to the high prohibitive price of this equipment. Due to it, optimization procedures are required to develop competitive

and efficient SIC-SFCL. Consequently, the literature presents several ways to optimize this equipment.

In [30], the authors have proposed optimization of the open core SIC-SFCL, where the evolutionary algorithm was used to optimize the cost and the voltage drop produced by this equipment. In [31], the authors use the genetic algorithm to optimize the six iron core SIC-SFCL, where the electrical parameters are considered in the model.

In [24] Nuno et al. present a genetic algorithm, which found an optimal design of SIC-SFCL for a particular power grid with specific parameters. Moreover, in this method, decision variables are implemented, and they are:

- the cross-section area of the DC limb,
- mean magnetic length of the limbs,
- number of turns of AC coils,
- mean magnetic length of the yokes.

The DC current is considered as a constant, and the number of turns of the DC coil is considered to track the optimal bias magnetomotive force, which saturates all iron cores. Furthermore, this methodology considers the magnetic circuit with the leaked inductance. The objective is to minimize the iron core volume.

In [6], dos Santos et al. have developed a method to optimize the superconducting bias coil and the applied DC superconducting coil. The optimization procedure utilizes the Nelder-Mead algorithm to solve the multi-objective optimization. As a result of the optimization, the optimal parameters are obtained, such as the number of turns and layers as well as the distance between them, the optimal current of the superconducting coil, etc. The methods use restrictions to control the optimization, and they are:

- critical current density,
- voltage drop in between the copper coil windings,
- normalization of current density,
- price of the HTS coil.

According to the last optimization results, it is possible to notice the influence of the magnetic leakage flux over the superconducting coil. Regarding this influence, the designer can choose the better position for the HTS coil.

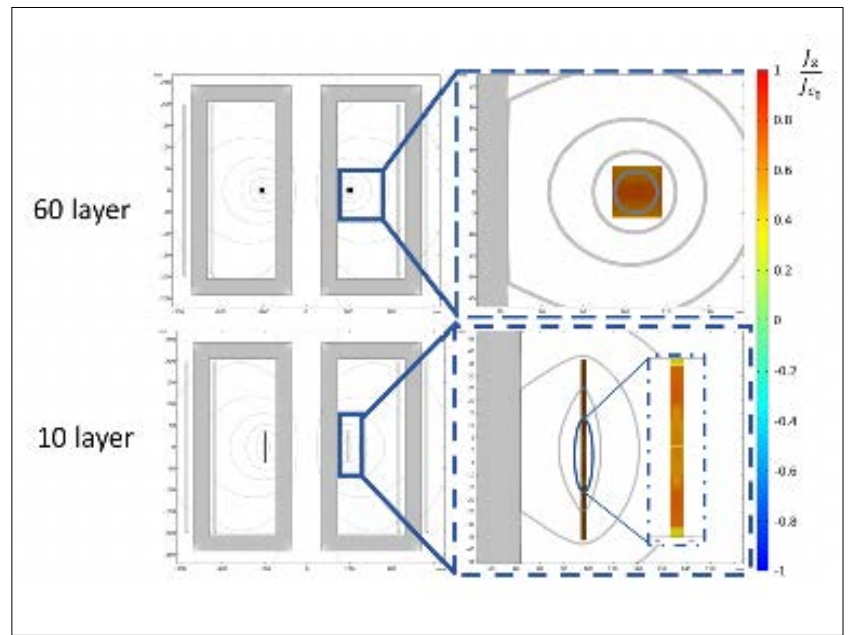


Figure 13. Current density (color map) and the magnetic flux line (gray lines)

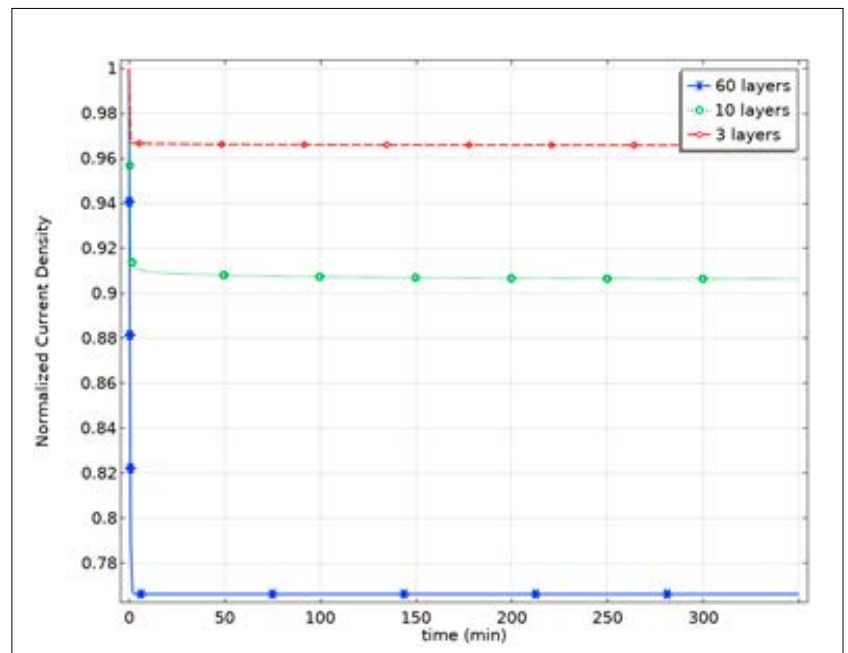


Figure 14. Normalized current density with different layers

For example, Fig. 13 illustrates the explanation above, wherein the normalized current density and the magnetic flux lines are considered for two different cases. In both, the applied direct current is equal to 250 A. Therefore, the changing of the normalized current density observed in Fig. 13 can be attributed to the different numbers of layers (60 and 10 layers). Moreover, in the 60 layers case, the magnetic flux is more perpendicular with regard to the tape. This situation needs to be avoided due to the high dependence of the critical current density regarding the perpendicular magnetic field.

Fig. 14 allows us to clarify the huge impact that the choice of the geometry can cause on the critical current density of the superconducting material. In these cases, the selection of 60 layers reduces the average of the critical current density to 76 % of the total normalized critical density of the material. On the other hand, as the number of layers decreases as normalized critical current density increases. This result shows that the reduction of the magnetic field over the HTS tapes is better if there are more stacks and fewer layers in the SIC-SFCL HTS coil configuration.

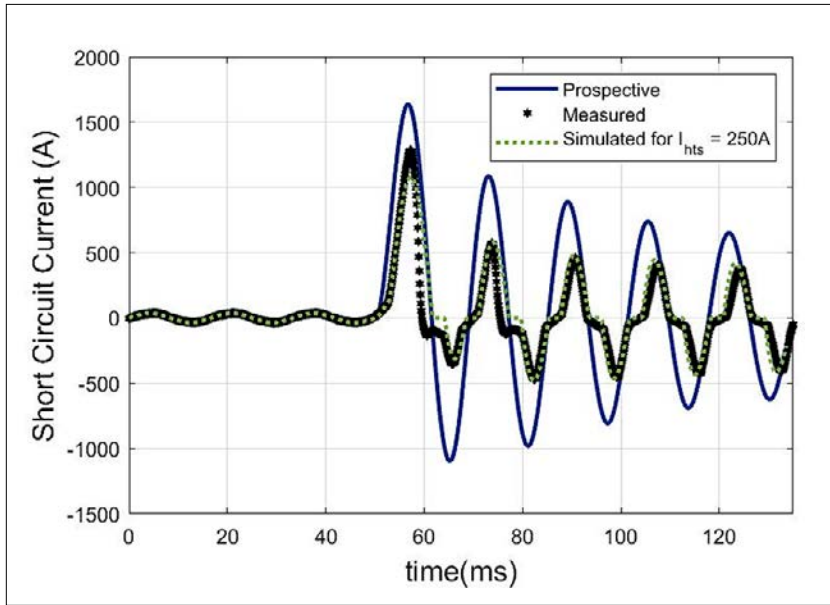


Figure 15. Short-circuit current with DC current equals 250 A

SIC-SFCL design optimization case study shows that the reduction of the magnetic field over the HTS tapes is better if there are more stacks and fewer layers in the SIC-SFCL HTS coil configuration

In this optimization method, article [6] shows the minimum possible fill factor might not be the best choice to wound the DC bias coil, furthermore utilizing this methodology is possible to find the optimal DC current applied in the HTS coil. Moreover, in [5], [6], the authors have studied transient behavior of this kind of SIC-SFCL at the short-circuit regime presented in Fig. 15, where the problem was solved by the COMSOL package. In this case, it is possible to see the first peak reduction of around 20 %. The low limitation of this fault current limiter is justified by the time iron cores take to desaturate and change the impedance that the system observes.

In order to classify and compare the kinds of FCL, some operational aspects are limitation capability, relative cost, recovery time, safe fail, and steady-state losses. Table 1 summarizes the qualitative comparison among the FCLs. This table is classifying them into High, Moderate, and Low. Where “High” is the best aspect related to the other FCLs and “Low” is the worst one for that aspect.

Table 1. Comparison between the aspect of different kinds of FCL

FLC Type	Aspect				
	Limitation Capability	Relative cost	Recovery Time	Safe Failure	Study State Losses
Air-core reactor	Low	High	High	High	Low
Pyrotechnic FCL	High	Low	Low	Low	Moderate
Resistive superconducting	Moderate	Low	Low	High	High
Saturated iron core	Low	Low	High	High	Low
Shielded core reactor	Moderate	Low	Low	High	Moderate
Series switched reactor	High	Moderate	High	High	Moderate
Resonant circuit	Moderate	Moderate	High	Low	Moderate
Solid state bridge	Moderate	High	High	Low	Moderate
Hybrid FCL	High	Low	Moderate	High	High

Efforts to study the design, manufacturing, and optimization procedures of the SIC-SFCL are required to make this technology become available and competitive on the market

Conclusion

This article has presented and discussed different topologies of the SIC-SFCL and their advantages and disadvantages. Moreover, this article presents the principal parts that comprise a SIC-SFCL, where each component's physical and practical aspects were emphasized. After the recovery time of the SIC-SFCL is discussed, the influences of different iron core materials over the re-saturation processes are presented. In addition, the impact of the DC current shape in the transient period of the re-saturation is discussed. Several optimization procedures were presented and discussed in section 4. Moreover, in this section, the influence of the geometry of the DC HTS coil in the critical current density was discussed.

Among the superconducting fault current limiters presented in the literature, the SIC-SFCL has high maturity having several applications on the real substations of 35 kV/90 MVA, 220 kV/300 MVA, or 500 kV. Therefore, this equipment can become industrial. Efforts to study the design, manufacturing, and optimization procedures are required for this technology to become available and competitive on the market.

Bibliography

- [1] M. R. Barzegar-Bafrooei, A. A. Foroud, J. D. Ashkezari et al., *On the advance of SFCL: a comprehensive review*, IET Gener. Transm. Distrib., vol. 13, no. 17, pp. 3745–3759, 2019, doi: <https://doi.org/10.1049/iet-gtd.2018.6842>
- [2] G. Zhang, H. Wang, Q. Qiu et al., *Recent progress of superconducting fault current limiter in China*, Supercond. Sci. Technol., vol. 34, no. 1, p. 013001, Nov. 2020, doi: [10.1088/1361-6668/abac1f](https://doi.org/10.1088/1361-6668/abac1f)
- [3] J. Yuan, P. Gan, Z. Zhang, et al., *Saturated-core fault current limiters for AC power systems: Towards reliable, economical and better performance application*, High Volt., vol. 5, no. 4, pp. 416–424, 2020, doi: <https://doi.org/10.1049/hve.2019.0049>
- [4] G. dos Santos et al., *Tests and recovery under load simulations of a novel bifilar resistive SFCL having undulated shape configuration*, Supercond. Sci. Technol., Jan. 2021, doi: [10.1088/1361-6668/abd9b6](https://doi.org/10.1088/1361-6668/abd9b6)
- [5] G. dos Santos, F. G. R. Martins, F. Sass et al., *A coupling method of the superconducting devices modeled by finite element method with the lumped parameters electrical circuit*, Supercond. Sci. Technol., vol. 34, no. 4, p. 045014, Mar. 2021, doi: [10.1088/1361-6668/abe600](https://doi.org/10.1088/1361-6668/abe600)
- [6] G. dos Santos, F. Sass, G. G. Sotelo, *Multi-objective optimization for the superconducting bias coil of a saturated iron core fault current limiter using the T-A formulation*, Supercond. Sci. Technol., vol. 34, no. 2, p. 025012, Jan. 2021, doi: [10.1088/1361-6668/abc8cf](https://doi.org/10.1088/1361-6668/abc8cf)
- [7] Y. Xin et al., *Field tests on a 35 kV/90 MVA Superconducting Fault Current Limiter*, in 2010 International Conference on Power System Technology, Oct. 2010, pp. 1–5, doi: [10.1109/POWERCON.2010.5666578](https://doi.org/10.1109/POWERCON.2010.5666578)
- [8] *HTS dc bias coil for 35 kV/90 MVA saturated iron-core fault current limiter* - ScienceDirect, <https://www.science-direct.com/science/article/abs/pii/S0921453408004358> (accessed 19 Mar 2021)
- [9] Y. Xin et al., *Manufacturing and test of a 35 kV/90 MVA saturated iron-core type superconductive fault current limiter for live-grid operation*, IEEE Trans. Appl. Supercond., vol. 19, no. 3, pp. 1934–1937, Jun. 2009, doi: [10.1109/TASC.2009.2018510](https://doi.org/10.1109/TASC.2009.2018510)
- [10] Y. Xin et al., *Performance of the 35 kV/90 MVA SFCL in Live-grid fault current limiting tests*, IEEE Trans. Appl. Supercond., vol. 21, no. 3, pp. 1294–1297, Jun. 2011, doi: [10.1109/TASC.2011.2105452](https://doi.org/10.1109/TASC.2011.2105452)
- [11] H. Xiao et al., *Analysis of Transient Overvoltage in 220 kV Saturated Core HTS FCL*, IEEE Trans. Magn., vol. 47, no. 10, pp. 2620–2623, Oct. 2011, doi: [10.1109/TMAG.2011.2158575](https://doi.org/10.1109/TMAG.2011.2158575)
- [12] Y. Xin et al., *Development of a 220 kV/300 MVA superconductive fault current limiter*, Supercond. Sci. Technol., vol. 25, no. 10, p. 105011, Aug. 2012, doi: [10.1088/0953-2048/25/10/105011](https://doi.org/10.1088/0953-2048/25/10/105011)
- [13] Y. Xin et al., *Factory and field tests of a 220 kV/300 MVA statured iron-core superconducting fault current limiter*, IEEE Trans. Appl. Supercond., vol. 23, no. 3, pp. 5602305–5602305, Jun. 2013, doi: [10.1109/TASC.2012.2234205](https://doi.org/10.1109/TASC.2012.2234205)
- [14] B. Yang, L. Jing, W. Wei, *Based on the Ansoft 500 kV SICSFCL simulation analysis*, in 2017 4th International Conference on Information Science and Control Engineering (ICISCE), Jul. 2017, pp. 883–886, doi: [10.1109/ICISCE.2017.187](https://doi.org/10.1109/ICISCE.2017.187)
- [15] C. Li et al., *Cooling unit for the 500 kV Saturated iron core fault current limiter*, IEEE Trans. Appl. Supercond., vol. 29, no. 5, pp. 1–5, Aug. 2019, doi: [10.1109/TASC.2019.2897714](https://doi.org/10.1109/TASC.2019.2897714)
- [16] T. Ma, S. Dai, M. Song et al., *Electromagnetic Design of high-temperature superconducting DC Bias winding for single-phase 500 kV Saturated iron-core fault current limiter*, IEEE Trans. Appl. Supercond., vol. 28, no. 3, pp. 1–5, Apr. 2018, doi: [10.1109/TASC.2017.2777877](https://doi.org/10.1109/TASC.2017.2777877)
- [17] M. Yu, H. Hong, H. Chen, *Electromagnetic transient simulation analysis for the 500 kV saturated iron-core superconducting fault current limiter*, in 2019 IEEE Innovative Smart Grid Technologies - Asia (ISGT Asia), May 2019, pp. 2613–2618, doi: [10.1109/ISGT-Asia.2019.8881196](https://doi.org/10.1109/ISGT-Asia.2019.8881196)
- [18] C. Liang et al., *Winding technology and experimental study on 500 kV superconductive fault current limiter*,

IEEE Trans. Appl. Supercond., vol. 28, no. 3, pp. 1–5, Apr. 2018, doi: 10.1109/TASC.2018.2805722

[19] P. A. Commins, J. W. Moscrop, *Analytical Nonlinear reluctance model of a single-phase saturated core fault current limiter*, IEEE Trans. Power Deliv., vol. 28, no. 1, pp. 450–457, Jan. 2013, doi: 10.1109/TPWRD.2012.2214404

[20] A. Pellecchia et al., *Development of a saturated core fault current limiter with open magnetic cores and magnesium diboride saturating coils*, IEEE Trans. Appl. Supercond., vol. 27, no. 4, pp. 1–7, Jun. 2017, doi: 10.1109/TASC.2016.2642147

[21] J. Cabanes Aracil, J. Lopez-Roldan, J. C. Coetzee et al., *Analysis of electromagnetic forces in high voltage superconducting fault current limiters with saturated core*, Int. J. Electr. Power Energy Syst., vol. 43, no. 1, pp. 1087–1093, Dec. 2012, doi: 10.1016/j.ijepes.2012.05.043

[22] P. A. Commins, J. W. Moscrop, *Three phase saturated core fault current limiter performance with a floating neutral*, in 2012 IEEE Electrical Power and Energy Conference, Oct. 2012, pp. 249–254, doi: 10.1109/EPEC.2012.6474960

[23] J. C. Knott, P. A. Commins, J. W. Moscrop et al., *Design considerations in MgB₂-based superconducting coils for use in saturated-core fault current limiters*, IEEE Trans. Appl. Supercond., vol. 24, no. 5, pp. 1–4, Oct. 2014, doi: 10.1109/TASC.2014.2340459

[24] N. Vilhena, P. Arsénio, J. Murta-Pina et al., *A methodology for modeling and simulation of saturated cores fault current limiters*, IEEE Trans. Appl. Supercond., vol. 25, no. 3, pp. 1–4, Jun. 2015, doi: 10.1109/TASC.2014.2374179

[25] *Application studies on the active SISFCL in electric transmission system and its impact on line distance protection*, IEEE Journals & Magazine, IEEE Xplore, <https://ieeexplore.ieee.org/document/6949111> (accessed 19 Mar. 2021)

[26] D. Cvoric, S. W. H. de Haan, J. A. Ferreira, *New saturable-core fault current*

limiter topology with reduced core size, in 2009 IEEE 6th International Power Electronics and Motion Control Conference, May 2009, pp. 920–926, doi: 10.1109/IPEMC.2009.5157515

[27] H. Hong et al., *DC magnetization system for a 35 kV/90 MVA superconducting saturated iron-core fault current limiter*, IEEE Trans. Appl. Supercond., vol. 19, no. 3, pp. 1851–1854, Jun. 2009, doi: 10.1109/TASC.2009.2019292

[28] B. Shen et al., *Investigation on power dissipation in the saturated iron-core superconducting fault current limiter*, IEEE Trans. Appl. Supercond., vol. 29, no. 2, pp. 1–5, Mar. 2019, doi: 10.1109/TASC.2018.2881706

[29] F. Trillaud, G. dos Santos, G. Gonçalves Sotelo, *Essential material knowledge and recent model developments for rebco-coated conductors in*

electric power systems, Materials, vol. 14, no. 8, Art. no. 8, Jan. 2021, doi: 10.3390/ma14081892

[30] J. C. Aracil, J. Lopez-Roldan, J. C. Coetzee et al., *Saturated core high-temperature superconducting fault current limiters as an alternative to conventional series reactors in a distribution grid*, in 10th IET International Conference on AC and DC Power Transmission (ACDC 2012), Dec. 2012, pp. 1–6, doi: 10.1049/cp.2012.1997

[31] A. Dey, A. B. Choudhury, *A comparative study between scalarization approach and Pareto approach for multi-objective optimization problem using Genetic Algorithm (MOGA) formulated based on superconducting fault current limiter*, in 2016 IEEE 1st International Conference on Power Electronics, Intelligent Control and Energy Systems (ICPEICES), Jul. 2016, pp. 1–4, doi: 10.1109/ICPEICES.2016.7853238

Authors



Gabriel dos Santos is a PhD student in Electrical Engineering at Universidade Federal Fluminense. He has acquired a master's degree in Electrical Engineering at Universidade Federal Fluminense (2021). He graduated in Electrical Engineering from the Federal University of Rio de Janeiro in 2019. His research areas are power electronics, simulations of electromagnetic machines and devices, renewable energy sources, electromagnetic transients, simulations of electrical machines using finite element and finite difference methods, dimensioning and automation of orienting systems, photovoltaic systems, modeling, development, and manufacture of superconducting equipment and designs of superconducting short-circuit limiters and power electronics.



Guilherme G. Sotelo was born in Rio de Janeiro, Brazil. He received the M.Sc. and Ph.D. degrees in electrical engineering from the Federal University of Rio de Janeiro in 2003 and 2007, respectively. He was an Assistant Professor from 2009 to 2017 and is currently an Associate Professor with the Department of Electrical Engineering, Fluminense Federal University, Niteroi, Brazil, working on superconducting electric power applications.



Felipe Sass received the M.Sc. (2011) and Ph.D. (2015) in electrical engineering from the Federal University of Rio de Janeiro. He is currently a Professor with the Department of Electrical Engineering at Fluminense Federal University, where he graduated in 2008. His current research interests include industrial applications, superconducting devices, and embedded systems.